IEEE Photonics Journal
An IEEE Photonics Society Publication

Open Access

A Novel Plasmonic Sensor Based on Metal–Insulator–Metal Waveguide With Side-Coupled Hexagonal Cavity

Volume 7, Number 2, April 2015

Yi-Yuan Xie
Ye-Xiong Huang
Wei-Lun Zhao
Wei-Hua Xu
Chao He

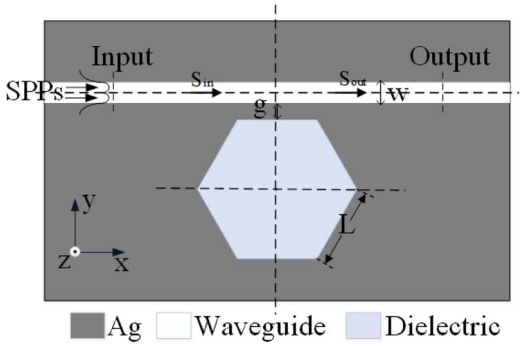

DOI: 10.1109/JPHOT.2015.2419635
1943-0655

A Novel Plasmonic Sensor Based on Metal–Insulator–Metal Waveguide With Side-Coupled Hexagonal Cavity

Yi-Yuan Xie, Ye-Xiong Huang, Wei-Lun Zhao, Wei-Hua Xu, and Chao He

School of Electronic and Information Engineering, Southwest University, Chongqing 400715, China

DOI: 10.1109/JPHOT.2015.2419635

Manuscript received March 11, 2015; revised March 29, 2015; accepted March 31, 2015. Date of publication April 8, 2015; date of current version April 20, 2015. This work was supported in part by the National Natural Science Foundation of China under Grant 61205088, by the Natural Science Foundation of Chongqing Municipal under Grant 2011BB2009, by the Fundamental Research Funds for the Central Universities under Grant XDJK2014A017, and by the 863 Program of China under Grant 2015AA016300. Corresponding author: Y.-Y. Xie (e-mail: yyxie@swu.edu.cn).

Abstract: We propose a novel and compact plasmonic sensing structure based on a metal–insulator–metal (MIM) waveguide with a side-coupled hexagonal cavity. The sensing structure has been numerically and theoretically investigated using the finite-difference time-domain (FDTD) method and temporal coupled-mode theory. The numerical simulation results show that the resonance dips of the structure have a high resonant transmission contrast ratio and that the resonance wavelengths have a near-linear relationship with the refractive index of the dielectric material in the cavity. The numerical simulation results obtained from the transmission spectra are used to analyze the sensing characteristic of the structure. The effects of the geometrical parameters on the transmission and sensing characteristics of the structure are analyzed in detail. The sensitivity can be tuned to a value as high as 1562.5 nm per refractive-index unit (RIU) with a high figure of merit of $\sim$38.6 RIU^{-1} around the resonance wavelength of 1550 nm using the novel structure and by optimizing the structural parameters. In addition, the temperature-sensing characteristic of the structure based on the refractive-index sensor is also discussed in this paper. The proposed structure may potentially be applied in optical networks-on-chip and on-chip nanosensors.

Index Terms: Plasmonic sensor, metal–insulator–metal (MIM) waveguide, hexagonal cavity, finite-difference time-domain (FDTD) method.

1. Introduction

Surface plasmon polaritons (SPPs), which are surface electromagnetic waves excited at the metal–dielectric interfaces, have many advantages, including overcoming the diffraction limit of light waves and guiding light waves at subwavelength scales. They are, therefore, considered to be promising energy and information carriers and have been used to the realization of highly integrated optical devices and circuits [1]–[6]. Over the past few years, SPPs have become a very attractive subject of research for the construction of subwavelength optical devices, and numerous devices with different structures based on SPPs have been proposed and numerically investigated [7]–[16]. Among the plasmonic waveguide structures, metal–insulator–metal (MIM) waveguide, composed of two metallic claddings and a dielectric core, has

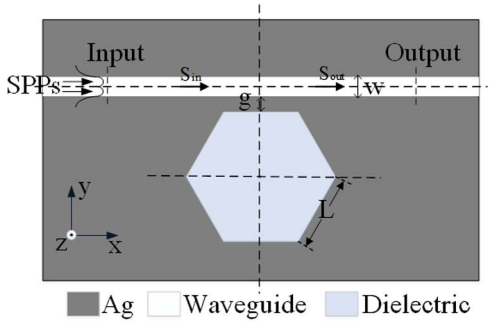

Fig. 1. Schematic diagram of the plasmonic sensor based on a MIM waveguide with a laterally coupled hexagonal cavity.

received special attention for guiding SPPs at subwavelength scales owing to its strong light confinement, acceptable propagation length, low bend loss, and relative ease fabrication [17]. Accordingly, theoretical results on MIM waveguide-based plasmonic devices and their applications have been reported. Their applications include filters [7]–[9], demultiplexers [10]–[13], splitters [14], all-optical switches [15], and all-optical logic gates [16]. An optical sensor, one of the most important devices in sensing applications, has significant advantages such as immunity to electromagnetic interference, great sensitivity, and a wide dynamic range [18]. Optical sensors based on surface plasmon resonance (SPR) used for detecting refractive index changes of materials have received great attention for their unique optical properties including local electromagnetic field enhancement and ultra-sensitivity of the SPR to the surrounding medium [19]–[21]. However, traditional SPR sensors are not suitable for integration. SPR sensors based on SPPs have received great attention, owing to the distinguished advantages of SPPs, to alleviate issues of high integration and high sensitivity. In the recent years, efforts have been made to investigate plasmonic sensors based on MIM waveguides or waveguide-coupled structures, and many new kinds of SPP sensors have been proposed and numerically investigated to achieve the goals stated above. These sensors include a tooth-shaped structure [22], an MIM waveguide with a single defect [23], plasmonic waveguides with ring resonators [24], [25], a slot cavity [26], and a nanodisk resonator [27]. In these structures, the plasmonic resonator is the critical element that influences the transmission and sensing characteristics of the devices. To improve the performance of the plasmonic MIM waveguide-based sensors, for the first time to the best of our knowledge, a hexagonal cavity has been used to construct the plasmonic sensing structure in this study. The structure is composed of an MIM waveguide and a laterally coupled hexagonal cavity. Compared to a structure based on a nanodisk cavity, the interaction length of the proposed sensing structure is much longer. The FDTD method and temporal coupled-mode theory have been used to numerically and theoretically investigate the transmission and sensing characteristics of the sensing structure. These results lay the theoretical foundation for designing compact sensors in optical networks-on-chip and on-chip nanosensors.

2. Structure Model and Theoretical Analysis

Fig. 1 shows a 2-D schematic of the proposed structure of the plasmonic sensor, which is composed of an MIM waveguide and a laterally coupled hexagonal cavity. The structure parameter L is the side length of the hexagonal cavity and the interaction length between the MIM waveguide and the hexagonal cavity. w is the width of the MIM waveguide. g is the coupling distance between the boundary of the hexagonal cavity and the MIM waveguide. S_{in} represents the amplitude of incident light, whereas S_{out} represents the amplitude of the transmitted light. The MIM waveguide medium is set as air, with a refractive index of $n = 1$. The hexagonal cavity is filled with the dielectric material of refractive index n_d. The selected metal is silver owing to its low

ohmic loss, and its frequency-dependent permittivity can be characterized by the Lorentz–Drude model [28]:

$$\varepsilon_m(\omega) = \varepsilon - \sum_{i=1}^{6} \frac{\omega_{p,i}^2}{\left(\omega_{a,i}^2 - \omega^2 + i\omega\omega_{c,i}\right)} \tag{1}$$

where ε, ω_a, ω_c, ω_p, and ω represent the relative dielectric constant at infinite frequency, the resonance frequency, the damping frequency, the plasma frequency, and the angular frequency of the incident wave, respectively.

Since the width of the MIM waveguide is much smaller than the incident wavelength, the SPPs waves are only excited by the fundamental transverse magnetic (TM) mode in the MIM waveguide. As shown in the figure, the SPPs waves are excited by TM mode on the left side of the waveguide and propagate along the MIM waveguide from the input port to the output port. The dispersion relation of the fundamental TM mode in the MIM waveguide can be obtained by the following equations [11]:

$$(\varepsilon_m k_d)\tanh\left(\frac{wk_d}{2}\right) + \varepsilon_d k_m = 0 \tag{2}$$

$$k_d = \sqrt{\beta^2 - \varepsilon_d k_0^2} \tag{3}$$

$$k_m = \sqrt{\beta^2 - \varepsilon_m k_0^2} \tag{4}$$

$$n_{eff} = \beta / k_0 \tag{5}$$

where ε_m and ε_d are the dielectric constants, and k_m, k_d are the propagation constants in the metal and insulator, respectively. The propagation constant of the SPP waves is denoted by β. The expression $k_0 = 2\pi/\lambda$ represents the wave number of the incident light with wavelength λ in vacuum. The effective refractive index in the MIM waveguide, n_{eff}, includes a real part $(\mathrm{Re}(n_{eff}))$ and an imaginary part $(\mathrm{Im}(n_{eff}))$. Generally, the imaginary part can be neglected because it is small and only affects the propagation length of SPPs. According to (2)–(5), the effective refractive index is relevant with the width of the MIM waveguide. In fact, the real part $\mathrm{Re}(n_{eff})$ decreases as the width of the MIM waveguide increases for a certain wavelength of light, and then declines slowly as the incident wavelength increases for a certain width of the waveguide [29].

When a wave propagates along the MIM waveguide from the input port to the output port, part of the energy couples to the hexagonal cavity through the interaction length between the MIM waveguide and the hexagonal cavity. Since the structure consists of a waveguide and a side-coupled cavity, the transmission characteristics of the structure can be analyzed by the temporal coupled-mode theory [30], [31]. The temporal evolution of the normalized amplitude A of the cavity may be given as

$$\frac{dA}{dt} = (j\omega_r - k_o - k_e)A + \sqrt{k_e}e^{j\theta}S_{in} \tag{6}$$

where ω_r is the resonance frequency of the cavity, and k_o denotes the decay rate of the field due to internal loss in the cavity, whereas k_e denotes the decay rate of the field due to the energy coupled into the waveguide. If S_{in} has a time dependence of $e^{j\omega t}$, we can deduce from (6) that at steady state

$$A = \frac{\sqrt{k_e}e^{j\theta}S_{in}}{j(\omega - \omega_r) + k_o + k_e} \tag{7}$$

where θ is the phase of the coupling coefficients between the cavity and the waveguide. By energy conservation, the output light may be described as

$$S_{out} = S_{in} - \sqrt{k_e}e^{-j\theta}A \tag{8}$$

The transmission characteristic T_r of the structure may then be obtained based on the above equations:

$$T_r = \left|\frac{s_{+,out}}{s_{in}}\right|^2 = \frac{(\omega-\omega_r)^2 + k_o^2}{(\omega-\omega_r)^2 + (k_o+k_e)^2}. \tag{9}$$

At the resonance frequency, a standing wave may be formed in the cavity, producing a resonance dip in the transmission spectrum with a minimal value of T_{rmin}. From (9), we obtain

$$T_{r\min} = k_o^2/(k_o+k_e)^2. \tag{10}$$

For the SPP cavity, the resonance condition may be given by

$$m \cdot 2\pi = \frac{2\pi}{\lambda_m}(6L)\mathrm{Re}(N_{eff}) + \varphi \tag{11}$$

where λ_m is the resonance wavelength, N_{eff} is the effective index of the cavity for SPPs, that is dependent on the refractive index n_d, m is a positive integer, corresponding to the number of antinodes of the standing wave in the cavity, and φ represents the total phase shift at the corners of the hexagonal cavity. From (11), it is apparent that the resonance wavelength is related to the refractive index of the dielectric and the side length of the hexagonal cavity.

According to (9), the FWHM of the resonance wavelength can be derived as

$$\Delta\lambda_{FWHM} = \frac{4\pi c(k_o+k_e)}{\omega_r^2}. \tag{12}$$

According to (10) and (12), it can be seen that the value of T_{rmin} and FWHM of the resonance wavelength are mainly dependent on the decay rates of the field, k_o and k_e.

Based on the above analysis, we note that the resonance wavelength is related to the refractive index of material. The refractive index is assumed to be related to the ambient temperature [32]

$$n = n_0 + dn/dT \cdot (T - T_0) \tag{13}$$

where n_0 is the refractive index of the sensing medium at the reference temperature T_0, and dn/dT represents the refractive index temperature coefficient. Equation (13) indicates that there is a linear relation between the refractive index and temperature, resulting in a similar relation between the temperature and the resonance wavelength. It implies that the temperature can be obtained by detecting the shift of the resonance wavelength. Therefore, a plasmonic sensor may be used to detect temperature. However, it requires a material with high refractive index temperature coefficient as the sensing medium to achieve high sensitivity.

3. Results and Discussions

To study the performance of the novel plasmonic sensor, we employed the FDTD method to simulate the structure. The black curve in Fig. 2(a) shows the transmission spectrum of the structure. Here, the structural parameters are set as $L = 450$ nm, $g = 15$ nm, $w = 50$ nm, and $n_d = 1.0$ so that the largest resonance wavelength could be obtained near 1550 nm. As can be seen, two very sharp resonance dips appear in the transmission spectrum at wavelengths of 1548 nm and 972.8 nm, corresponding to the first (mode1) and second (mode2) resonance modes, respectively. The resonance dips have transmittance values of about -18 dB and -23 dB and FWHM values of about 40.5 nm and 56.5 nm for mode1 and mode2, respectively. To compare the transmission characteristics of the structure based on the hexagonal cavity with a structure based on disk cavity, the transmission spectrum (blue curve) of the structure based on disk cavity is also shown in the Fig. 2(a). The corresponding resonance wavelengths appear at 1549 nm and 956 nm with transmittance values of about -4.1 dB and -6.9 dB and FWHM values of about 24 nm and 17.4 nm, respectively. According to the results, though the linewidth

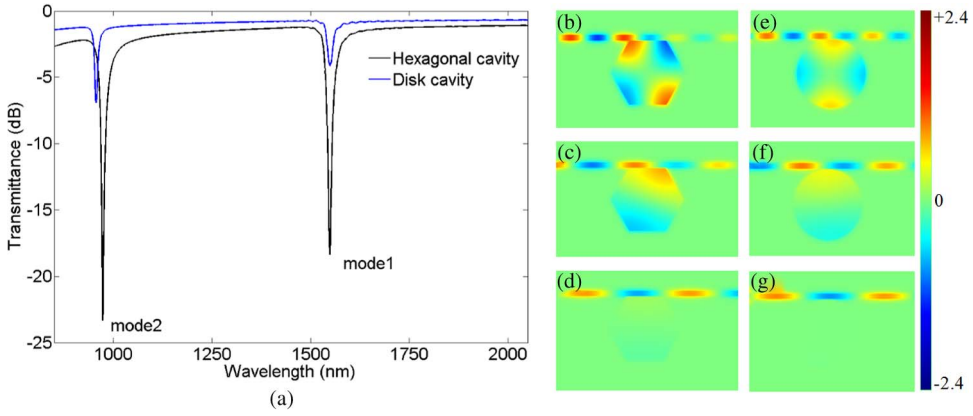

Fig. 2. (a) Simulated transmission spectra of the structures based on hexagonal cavity (black solid line) and disk cavity (blue solid line). Contour profiles of the field distributions of |Hz| for the structure based on hexagonal cavity at different incident wavelengths of (b) 972.8 nm, (c) 1548 nm, and (d) 2000 nm. The structure based on disk cavity at the different incident waves (e) 956 nm, (f) 1549 nm, and (g) 2000 nm.

of the resonance of the hexagonal cavity is larger than that of the structure based on disk cavity, the structure based on the hexagonal cavity has a much better resonant transmission contrast ratio. The resonant transmission contrast ratio is also an important parameter of the model, which may limit its applications [33]. To illustrate the performance difference between these two structures, the contour profiles of the field distributions of $|H_z|$ of the structure based on a hexagonal cavity for incident wavelengths of 972.8 nm, 1548 nm, and 2000 nm are shown in Fig. 2(b)–(d), respectively, whereas the contour profiles of the field distributions of $|H_z|$ of the structure based on a disk cavity for incident wavelengths of 956 nm, 1549 nm, and 2000 nm are shown in Fig. 2(e)–(g), respectively. As can be observed in Fig. 2(b)–(g), most of the energy of the incident waves is coupled to the cavities, and the corresponding standing waves are formed in the cavities at the resonance wavelengths. In these cases, almost no energy is propagated to the output port of the waveguide for destructive interference between the transmission field and the internal field coupled back into the output waveguide. At a wavelength of 2000 nm, the incident waves barely couple to the cavities and propagate to the output port of the MIM waveguide. These observations are consistent with the results from the transmission spectra. However, compared with the structure based on a disk cavity, as can be observed, more energy is coupled into the hexagonal cavity at the corresponding resonance wavelength. This means the coupling effect between the waveguide and the hexagonal cavity becomes stronger and results in much more energy coupling into the cavity. A stronger coupling effect implies a larger decay rate of the field due to the energy coupled into the waveguide. According to (10) and (12), this results in a higher resonant transmission contrast ratio and a much wider resonance linewidth than the structure based on a disk resonator.

Subsequently, we investigated the effects of structural parameters on the transmission characteristics of the structure to find an optimal set of parameters for the sensor. In order to study the influence of the waveguide width on the transmission characteristics, w was increased from 30 nm to 70 nm in 10-nm steps whereas other parameters were fixed at $L = 450$ nm, $g = 20$ nm, and $n_d = 1.0$. Fig. 3(a) and (b) shows the transmission spectra of the two modes for different waveguide widths. As can be observed in Fig. 3(a) and (b), the resonance wavelength exhibits a slight red-shift with an increasing waveguide width. In addition, increasing the width of the waveguide also affects the transmission and FWHM values of the resonance wavelength. Mode1, exhibits a relatively better performance with a transmittance value of -32.2 dB and an FWHM value of 41.5 nm at $w = 40$ nm, whereas a relatively better performance with a transmittance value of -31 dB and an FWHM value of 44 nm occurs at $w = 70$ nm for mode2. This may be due to waveguide loss. Increasing the width of the waveguide decreases the coupling of

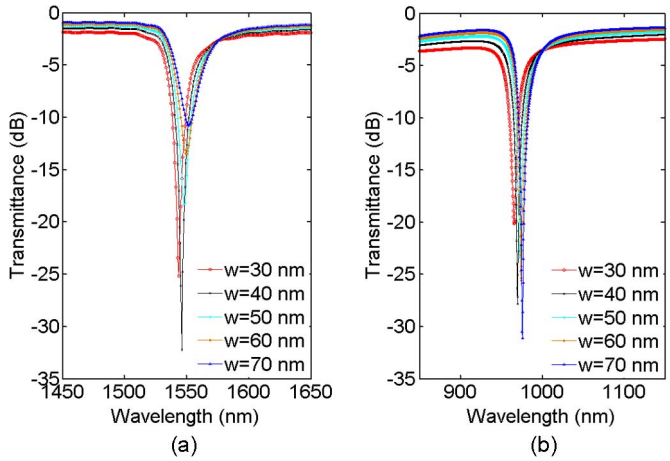

Fig. 3. Transmission spectra of the structure for different waveguide widths for (a) mode1 and (b) mode2.

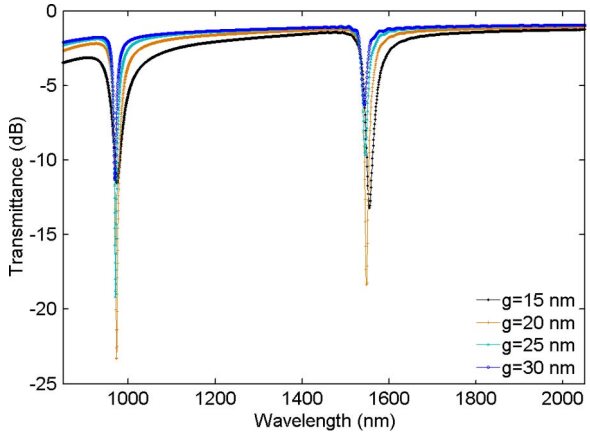

Fig. 4. Transmission spectra of the structure for different coupling distances between the waveguide and the cavity.

SPPs and reduces the waveguide loss. The decrease of the waveguide loss affects the coupling between the waveguide and the hexagonal cavity and thereby the transmission characteristic.

To analyze the effect of coupling distance on the transmission characteristics, g was increased from 10 nm to 30 nm in 5-nm steps, whereas the other respective parameters were set as $L = 450$ nm, $w = 50$ nm, and $n_d = 1.0$. Fig. 4 shows the transmission spectra for different coupling distances. As shown in Fig. 4, all the resonance wavelengths of the two modes exhibit slight blue-shifts as the coupling distance increases. In addition, increasing the coupling distance also affects the transmission and FWHM values of the resonance wavelength. Relatively better performances with transmittance values of -18 dB and -23 dB, and FWHM values of 40.5 nm and 56.5 nm were observed for mode1 and mode2, respectively, at $g = 20$ nm. This may be explained by temporal coupled-mode theory. Increasing the coupling distance results in a weaker coupling and smaller decay rate of the field due to the energy coupled into the waveguide. Therefore, according to (10) and (12), a change in the coupling distance affects the transmittance and FWHM of the resonance wavelength.

To further investigate the performance of the novel plasmonic sensor, we have also studied the effect of the side length L on the transmittance characteristics. The side length L was increased from 410 nm to 490 nm in steps of 10 nm whereas other parameters were set at $g = 20$ nm, $w = 50$ nm, and $n_d = 1.0$. Fig. 5(a) shows the transmission spectra of the sensor for

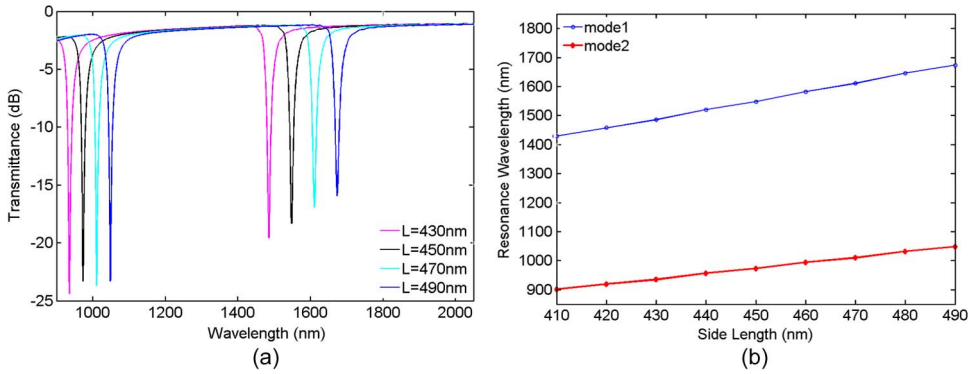

Fig. 5. (a) Transmission spectra of the structure for different side lengths. (b) Resonance wavelength as a function of the side length L.

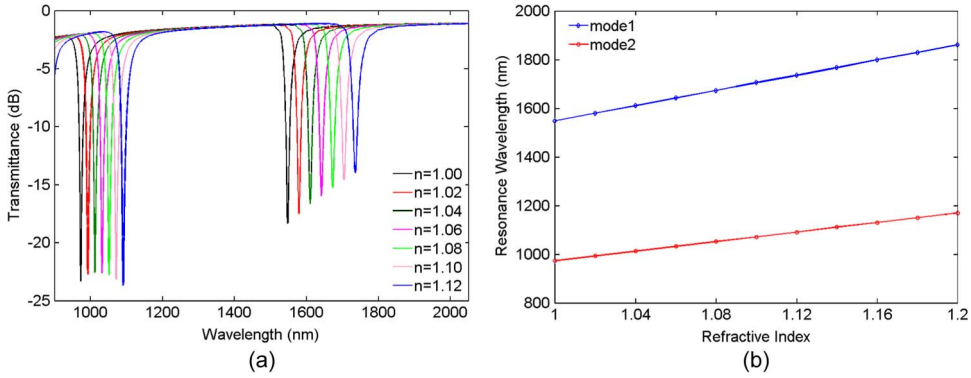

Fig. 6. (a) Transmission spectra of the structure with different refractive indices. (b) Resonance wavelength as a function of the refractive index of the dielectric in the cavity for the two modes.

different side lengths, where all the resonance wavelengths exhibit red-shifts with an increase in the side length. Fig. 5(b) shows an approximately linear relationship in the resonance wavelengths of the two modes as a function of the side length of the hexagonal cavity, which can be explained by (11). Therefore, one can tune the resonance wavelength by changing the side length of the hexagonal cavity. However, it has an insignificant influence on the transmission and FWHM at the resonance wavelength. The effect of the side length on the transmission characteristic at mode1 is larger than the effect at mode2. This may be due to weaker coupling at a larger wavelength.

In order to investigate the relationship between the refractive index of the dielectric in the cavity and its resonance wavelength, the refractive index of the cavity dielectric was increased from 1.0 to 1.2 in steps of 0.02, whereas the other parameters were fixed at $L = 450$ nm, $w = 50$ nm, and $g = 20$. Fig. 6(a) shows the resulting transmission spectra of the structure, where it may be observed, that all the resonance wavelengths exhibit a red-shift as the refractive index increases. Similar to the case of the side length, the transmittance decreases and FWHM increases with an increase in the refractive index for mode1. Fig. 6(b) shows linear relationships between the resonance wavelengths and the refractive indices for the two modes in the range of variation. Therefore, refractive index may be obtained by measuring the shift of a certain resonance wavelength based on its linear relationship. This is the sensing principle of the proposed structure as a sensor. Furthermore, for an SPR sensor, its sensitivity (S) and figure of merit (FOM) are important parameters to characterize its performance, and high values are preferred [19]–[21], [34]. The sensitivity of the sensor is defined as the shift in the resonance wavelength per unit variation of the refractive index $(S = \Delta\lambda/\Delta n)$ and FOM is

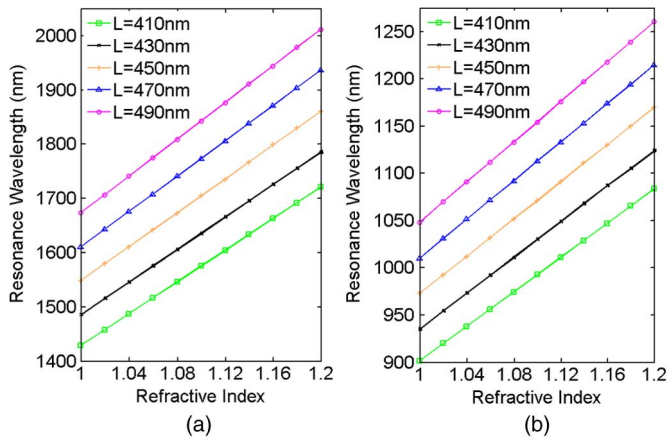

Fig. 7. Resonance wavelength of the structure as a function of the refractive index for different side lengths for (a) mode1 and (b) mode2.

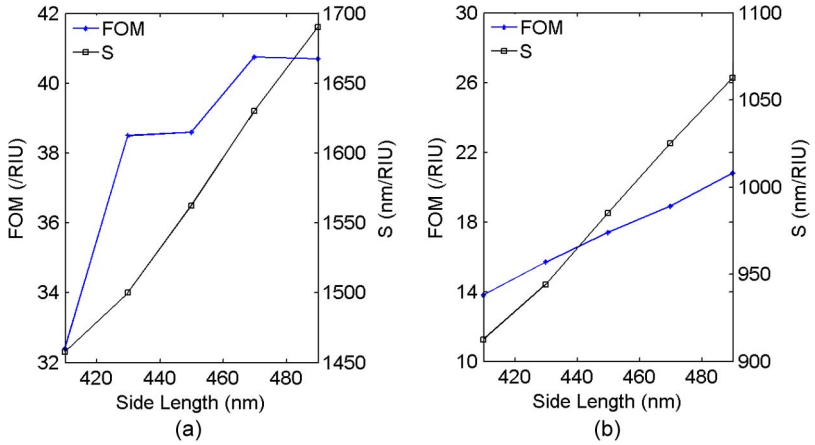

Fig. 8. Sensitivity and FOM as a function of the side length of the hexagonal cavity for (a) mode1 and (b) mode2.

obtained by dividing the sensitivity by the bandwidth of resonance [full width at half-maximum (FWHM)] ($FOM = S/\Delta\lambda_{FWHM}$). According to this definition, the sensitivity of the sensor can reach 1562.5 nm/RIU for mode1 and 985 nm/RIU for mode2. An FOM of $\sim$38.6 RIU^{-1} for mode1 and $\sim$17.4 RIU^{-1} for mode2, may be attained. Through the above analysis, it is clear that the proposed sensor not only has a high sensitivity, but a relatively high FOM value as well.

In order to improve the performance of the sensor, we also investigate how the structural parameters affect the sensing characteristics of the sensor. In order to illustrate the side length effects on the sensing characteristics of the structure, we changed the refractive index from 1.0 to 1.2 in steps of 0.02 for different side lengths of 410 nm, 430 nm, 450 nm, 470 nm, and 490 nm. Fig. 7(a) and (b) shows the relationship between the resonance wavelength and the refractive index for different side lengths for mode1 and mode2. Fig. 8(a) and (b) shows the sensitivity and FOM as functions of the side length. As can be observed, the sensitivity of the sensor almost increases linearly as the side length increases. As for the FOM, it increases linearly for mode2. In contrast to the FOM of mode2, the FOM of mode1 increases unsteadily and slowly after $L = 430$ nm as the side length increases. For example, the sensitivities are 1457.5 nm/RIU with an FOM of 32.4 RIU^{-1} for mode1 and 912.5 nm/RIU with an FOM of 13.8 RIU^{-1} for mode2 at $L = 410$ nm, and 1690 nm/RIU with an FOM of 40.7 RIU^{-1} for mode1

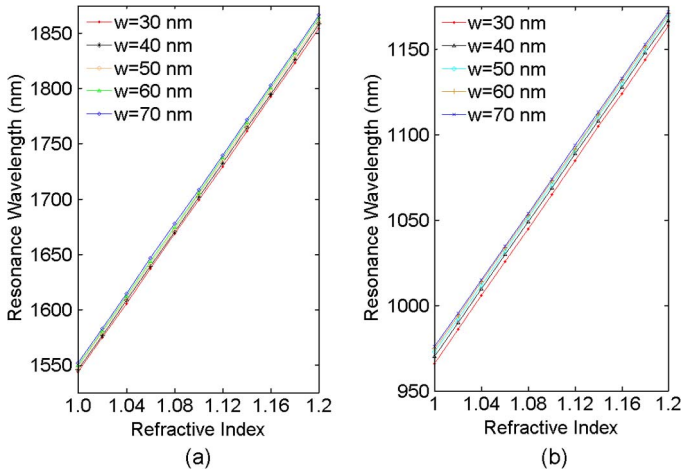

Fig. 9. Resonance wavelength of the structure as a function of refractive index for different waveguide widths for (a) mode1 and (b) mode2.

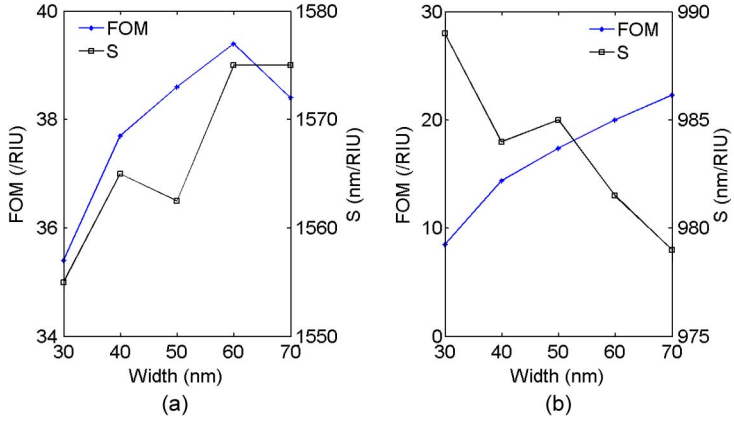

Fig. 10. Sensitivity and FOM as a function of width of waveguide for (a) mode1 and (b) mode2.

and 1062.5 nm/RIU with an FOM of 20.8 RIU^{-1} for mode2 at $L = 490$ nm. From the above analysis, the sensitivity and the FOM of the sensors can be tuned by changing the side length of the hexagonal cavity.

To investigate how the waveguide width w affects the sensing characteristics, we varied the waveguide widths from 30 nm to 70 nm in steps of 10 nm for different refractive indices, while keeping the other parameters fixed. Fig. 9(a) and (b) shows the relationship between the resonance wavelength and the refractive index for different waveguide widths for mode1 and mode2. Fig. 10 (a) and (b) shows the sensitivity and FOM as a function of the waveguide width. As can be observed, for mode1, the sensitivity increases and the FOM reaches its highest value at $w = 60$ nm with increasing waveguide width. Mode1 has the best sensitivity and FOM of 1575 nm/RIU and 39.4 RIU^{-1}, respectively, at $w = 60$ nm. For mode2, the FOM increases and the sensitivity decreases with increasing waveguide width. It has a relatively better FOM and sensitivity of 985 nm/RIU and 17.4 RIU^{-1}, respectively, at $w = 50$ nm. These results indicate that the sensitivity and FOM of the sensor can also be optimized by changing the waveguide width.

To discuss how the coupling distance affects the sensing characteristics, we used different coupling distances of 15 nm, 20 nm and 25 nm for different refractive indices, while keeping other parameters fixed. Fig. 11(a) and (b) shows the resonance wavelength versus the refractive index for different coupling distances for mode1 and mode2. As can be observed, the coupling

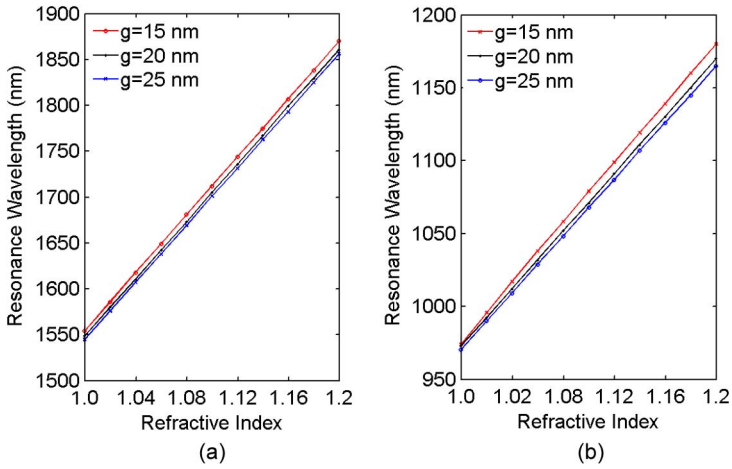

Fig. 11. Resonance wavelength of the structure as a function of refractive index for different coupling distances for (a) mode1 and (b) mode2.

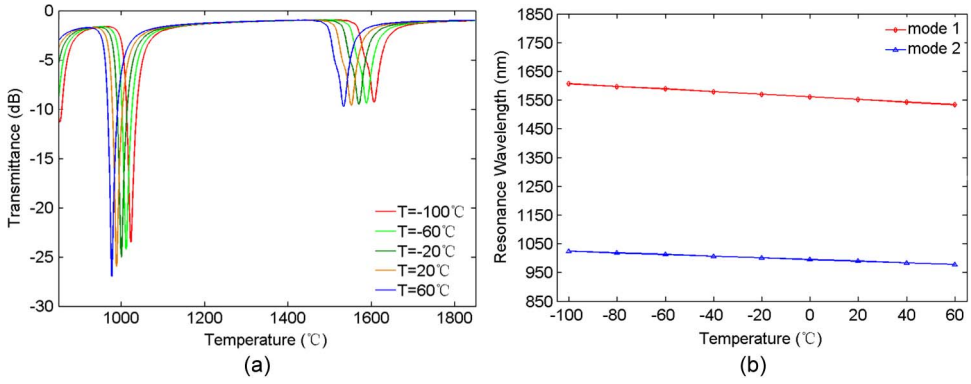

Fig. 12. (a) Transmission spectra of the structure for different temperatures. (b) Resonance wavelength as a function of the temperature for mode1 and mode2.

gap also influences the sensing characteristics of the structure. In these cases, the corresponding sensitivities are 1580 nm/RIU with an FOM of 25 RIU^{-1} for mode1 and 1030 nm/RIU with an FOM of 4.7 RIU^{-1} for mode2 at $g = 15$ nm, 1562.5 nm/RIU with an FOM of 38.6 RIU^{-1} for mode1 and 985 nm/RIU with an FOM of 17.4 RIU^{-1} for mode2 at $g = 20$ nm, and 1555 nm/RIU with an FOM of 50 RIU^{-1} for mode1 and 972 nm/RIU with an FOM of 28.6 RIU^{-1} for mode2 at $g = 25$ nm, respectively. Therefore, the sensitivity decreases while the FOM increases with an increase in coupling distance. In effect, the structure can also be optimized by changing the coupling distance.

Finally, we analyze the temperature-sensing characteristics of the proposed structure. In this work, we chose ethanol as the sensing medium that is filled in the hexagonal cavity, owing to its high refractive index temperature coefficient of 3.94×10^{-4} [24]. The complete relation between the refractive index n and the temperature T of ethanol is $n = 1.36836 - 3.94 \times 10^{-4} T$. In order to investigate the relationship between the resonance wavelength and the temperature, we increased the temperature of the medium from -100 °C to 60 °C in intervals of 20 °C according to the given relationship, whereas other structural parameters were set at be $L = 315$ nm, $g = 20$ nm, and $w = 50$ nm in order to obtain resonance wavelength near 1550 nm. Fig. 12(a) shows the transmission spectra for different temperatures. As shown in the figure, the resonance wavelength exhibits a blue shift as the temperature increases. This is because the

refractive index of ethanol decreases as the temperature increases. Fig. 12(b) shows a linear relationship between the resonance wavelength and temperature. The sensitivity of the temperature sensor is defined as $d\lambda/dT$, and using this, values of approximately 0.456 nm/°C for mode1 and 0.29 nm/°C for mode2 can be obtained, respectively. However, the sensitivities can be improved by controlling the structural parameters based on the above analysis. In particular, the temperature sensitivity can be evidently improved by increasing the side length of the hexagonal cavity. Therefore, the structure is appropriate for temperature sensing.

4. Conclusion

In conclusion, we have proposed a novel plasmonic sensor, which is composed of an MIM waveguide with a laterally coupled hexagonal cavity. The sensor has been investigated numerically and theoretically using the FDTD method and temporal coupled-mode theory. The simulated results show that the resonance wavelength has a high resonant transmission contrast ratio compared to that of the structure based on a disk cavity. The results also show a linear relationship with the refractive index of the dielectric in the hexagonal cavity. The sensitivity can reach values as high as 1562.5 nm/RIU with an FOM value of about $\sim$38.6 RIU^{-1} near the resonance wavelength of 1550 nm. Furthermore, the influence of the sensor's structural parameters on its transmission and sensing characteristics has been investigated in detail by analyzing the transmission spectra obtained. It has been shown that the sensor's sensitivity and FOM may be optimized by tuning the structural parameters. In addition, we have also investigated the temperature-sensing characteristics based on the refractive index sensing characteristics. Near the resonance wavelength of 1550 nm, the temperature sensitivity can reach 0.456 nm/°C. This sensor, with a compact and simple structure, may find many applications in optical networks-on-chip and on-chip nanosensors.

References

[1] W. L. Barnes, A. Dereux, and T. W. Ebbesen, "Surface plasmon subwavelength optics," *Nature*, vol. 424, no. 14, pp. 824–830, Aug. 2003.

[2] W. L. Barnes, "Surface plasmon-polariton length scales: A route to sub-wavelength optics," *J. Opt. A, Pure Appl. Opt.*, vol. 8, no. 4, pp. S87–S93, Apr. 2006.

[3] S. A. Maier and H. A. Atwater, "Plasmonics: Localization and guiding of electromagnetic energy in metal/dielectric structures," *J. Appl. Phys.*, vol. 98, no. 1, Jul. 2005, Art. ID. 011101.

[4] H. Ditlbacher, J. R. Krenn, G. Schider, A. Leitner, and F. R. Aussenegg, "Two-dimensional optics with surface plasmon polaritons," *Appl. Phys. Lett.*, vol. 81, no. 10, pp. 1762–1764, Sep. 2002.

[5] T. W. Ebbesen, C. Genet, and S. I. Bozhevolnyi, "Surface-plasmon circuitry," *Phys. Today*, vol. 61, no. 5, pp. 44–50, May 2008.

[6] D. K. Gramotnev and S. I. Bozhevolnyi, "Plasmonics beyond the diffraction limit," *Nat. Photon.*, vol. 4, no. 2, pp. 83–91, Feb. 2010.

[7] T. Wang, X. Wen, C. Yin, and H. Wang, "The transmission characteristics of surface plasmon polaritons in ring resonator," *Opt. Exp.*, vol. 17, no. 26, pp. 24 096–24 101, Dec. 2009.

[8] H. Lu, X. Liu, D. Mao, L. Wang, and Y. Gong, "Tunable band-pass plasmonic waveguide filters with nanodisk resonators," *Opt. Exp.*, vol. 18, no. 17, pp. 17 922–17 927, Aug. 2010.

[9] H. Lu, X. Liu, Y. Gong, L. Wang, and D. Mao, "Multi-channel plasmonic waveguide filters with disk-shaped nanocavities," *Opt. Commun.*, vol. 284, no. 10/11, pp. 2613–2616, May 2011.

[10] H. Lu, X. Liu, Y. Gong, D. Mao, and G. Wang, "Analysis of nanoplasmonic wavelength demultiplexing based on metal–insulator–metal waveguides," *J. Opt. Soc. Amer. B, Opt. Phys.*, vol. 28, no. 7, pp. 1616–1621, Jul. 2011.

[11] F. Lu, Z. Wang, K. Li, and A. Xu, "A plasmonic triple-wavelength demultiplexing structure based on MIM waveguide with side-coupled nanodisk cavities," *IEEE Trans. Nanotechnol.*, vol. 12, no. 6, pp. 1185–1189, Nov. 2013.

[12] G. Wang, H. Lu, X. Liu, D. Mao, and L. Duan, "Tunable multi-channel wavelength demultiplexer based on MIM plasmonic nanodisk resonators at telecommunication regime," *Opt. Exp.*, vol. 19, no. 4, pp. 3513–3518, Feb. 2011.

[13] H. Liu, Y. Gao, B. Zhu, G. Ren, and S. Jian, "A T-shaped high resolution plasmonic demultiplexer based on perturbations of two nanoresonators," *Opt. Commun.*, vol. 334, pp. 164–169, Jan. 2015.

[14] K. Wen *et al.*, "Design of an optical power and wavelength splitter based on subwavelength waveguides," *J. Lightw. Technol.*, vol. 32, no. 17, pp. 3020–3026, Sep. 2014.

[15] J. Tao, Q. Wang, and X. Huang, "All-optical plasmonic switches based on coupled nano-disk cavity structures containing nonlinear material," *Plasmonics*, vol. 6, no. 4, pp. 753–759, Aug. 2011.

[16] A. Dolatabady and N. Granpayeh, "All optical logic gates based on two dimensional plasmonic waveguides with nanodisk resonators," *J. Opt. Soc. Korea*, vol. 16, no. 4, pp. 432–442, Dec. 2012.

[17] A. Hosseini and Y. Massoud, "Nanoscale surface plasmon based resonator using rectangular geometry," *Appl. Phys. Lett.*, vol. 90, no. 18, Apr. 2007, Art. ID. 181102.
[18] G. D. Kim *et al.,* "Silicon photonic temperature sensor employing a ring resonator manufactured using a standard CMOS process," *Opt. Exp.*, vol. 18, no. 21, pp. 22 215–22 221, Oct. 2010.
[19] S. Roh, T. Chung, and B. Lee, "Overview of the characteristics of micro- and nano-structured surface plasmon resonance sensors," *Sensors*, vol. 11, no. 2, pp. 1565–1588, Jan. 2011.
[20] Y. Chen and H. Ming, "Review of surface plasmon resonance and localized surface plasmon resonance sensor," *Photon. Sens.*, vol. 2, no. 1, pp. 37–49, Oct. 2012.
[21] L. Tong, H. Wei, S. Zhang, and H. Xu, "Recent advances in plasmonic sensors," *Sensors*, vol. 14, no. 5, pp. 7959–7973, May 2014.
[22] J. Zhu, X. Huang, J. Tao, X. Jin, and X. Mei, "Nanometeric plasmonic refractive index senor," *Opt. Commun.*, vol. 285, no. 13/14, pp. 3242–3245, Jun. 2012.
[23] T. Wu *et al.,* "The sensing characteristics of plasmonic waveguide with a single defect," *Opt. Commun.*, vol. 323, pp. 44–48, Jul. 2014.
[24] T. Wu *et al.,* "The sensing characteristics of plasmonic waveguide with a ring resonator," *Opt. Exp.*, vol. 22, no. 7, pp. 7669–7677, Mar. 2014.
[25] S. Zou, F. Wang, R. Liang, L. Xiao, and M. Hu, "A nanoscale refractive index sensor based on asymmetric plasmonic waveguide with a ring resonator," *IEEE Sensors J.*, vol.15, no. 2, pp. 646–650, Feb. 2013.
[26] X. Jin, X. Huang, J. Tao, X. Lin, and Q. Zhang, "A novel nanometeric plasmonic refractive index sensor," *IEEE Trans. Nanotechnol.*, vol. 9, no. 2, pp. 134–137, Mar. 2010.
[27] A. Dolatabady, N. Granpayeh, and V. F. Nezhad, "A nanoscale refractive index sensor in two dimensional plasmonic waveguide with nanodisk resonator," *Opt. Commun.*, vol. 300, pp. 265–268, Jul. 2013.
[28] A. D. Rakic, A. B. Djurišic, J. M. Elazar, and M. L. Majewski, "Optical properties of metallic films for vertical-cavity optoelectronic devices," *Appl. Opt.*, vol. 37, no. 22, pp. 5271–5283, Aug. 1998.
[29] H. Shi *et al.,* "Beam manipulating by metallic nano-slits with variant widths," *Opt. Exp.*, vol. 13, no. 18, pp. 8815–6820, Sep. 2005.
[30] C. Manolatou *et al.,* "Coupling of modes analysis of resonant channel add–drop filters," *IEEE J. Quantum Electron.*, vol. 35, no. 9, pp.1322–1331, Sep. 1999.
[31] S. Xiao, L. Liu, and M. Qiu, "Resonator channel drop filters in a plasmon-polaritons metal," *Opt. Exp.*, vol. 14, no. 7, pp. 2932–2937, Apr. 2006.
[32] J. Hu, J. Chen, B. Liang, and Q. Jiang, "Influence of temperature on reflectivity of symmetrical metal-cladding optical waveguide,"*IEEE Photon. Technol. Lett.*, vol. 26, no. 21, pp. 2166–2169, Nov. 2014.
[33] Q. Huang, R. Liang, R. Chen, S. Wang, and Y. Xu, "High resonant transmission contrast filter based on the dual side-coupled cavities plasmonic structure," *J. Opt. Soc. Amer. B, Opt. Phys.*, vol. 28, no. 8, pp. 1851–1854, Aug. 2011.
[34] S. H. Kwon, "Deep subwavelength-scale metal–insulator–metal plasmonic disk cavities for refractive index sensors," *IEEE Photon. J.*, vol. 5, no. 1, Feb. 2013, Art. ID. 4800107.